JOC The Journal of Organic Chemistry

Article

pubs.acs.org/joc

Hydrothermal Photochemistry as a Mechanistic Tool in Organic Geochemistry: The Chemistry of Dibenzyl Ketone

Ziming Yang,[†] Edward D. Lorance,[‡] Christiana Bockisch,[†] Lynda B. Williams,*[,§] Hilairy E. Hartnett,*[,†,§] Everett L. Shock,*[,†,§] and Ian R. Gould*[,†]

[†]Department of Chemistry and Biochemistry, Arizona State University, Tempe, Arizona 85287, United States

[‡]Department of Chemistry, Vanguard University, Costa Mesa, California 92926, United States

[§]School of Earth and Space Exploration, Arizona State University, Tempe, Arizona 85287, United States

Supporting Information

ABSTRACT: Hydrothermal organic transformations under geochemically relevant conditions can result in complex product mixtures that form via multiple reaction pathways. The hydrothermal decomposition reactions of the model ketone dibenzyl ketone form a mixture of reduction, dehydration, fragmentation, and coupling products that suggest simultaneous and competitive radical and ionic reaction pathways. Here we show how Norrish Type I photocleavage of dibenzyl ketone can be used to independently generate the benzyl radicals previously proposed as the primary intermediates for the pure hydrothermal reaction. Under hydrothermal conditions, the benzyl radicals undergo hydrogen atom abstraction from dibenzyl ketone and *para*-coupling reactions that are not observed under ambient conditions. The photochemical method allows the primary radical coupling products to be identified, and because these products are generated rapidly, the method also allows the kinetics of the subsequent dehydration and Paal–Knorr cyclization reactions to be measured. In this way, the radical and ionic thermal and hydrothermal reaction pathways can be studied separately.

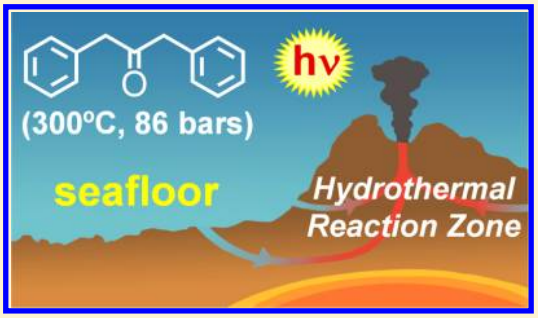

INTRODUCTION

Over 99.99% of the Earth's organic carbon does not actively participate in the biospheric carbon cycle but is located within the crust, mainly in continental and marine sedimentary basins in the form of kerogen.[1] It is estimated that more than 15 000 000 Gt of organic matter is located beneath the surface of the Earth.[1] The reactions of this huge quantity of organic matter contribute to a wide range of geochemically important processes. Reactions of organic material in the Earth's crust represent an important component of the deep (or geochemical) carbon cycle, which is an important factor in controlling atmospheric carbon dioxide levels.[2] Subsurface organic reactions are critical to petroleum generation and maturation processes,[3] can provide energy sources for deep microbial communities,[4] and have been implicated in the formation of ore deposits.[5]

From an organic chemistry perspective, it is interesting that the solvent for most of these reactions is water, usually at elevated temperatures and pressures.[6] Water at high temperatures and pressures is an excellent solvent for many organic reactions.[7−18] A wide range of reactions have now been identified in hot subcritical water (at associated confining pressures), which include fragmentations into smaller structures, additions to make larger structures, and functional group interconversions. These reactions take place in water without the addition of any external reagents or catalysts.[8] For these reasons, organic chemical reactions under conditions that mimic geochemical conditions are being studied as potential "green chemistry" systems.[9]

Many hydrothermal reactions are surprising compared with corresponding processes under ambient conditions. Examples include the endothermic elimination of hydrogen from alcohols and alkanes to form carbonyls and alkenes and the dehydration of alcohols to form alkenes.[8−12] Alcohol dehydration is particularly surprising since water is the solvent. The equilibrium between alcohol and alkene + water is strongly temperature-dependent, and for butanol the equilibrium is on the side of butene + water at temperatures above 200 °C at the vapor–liquid saturation pressure of water.[5] At higher temperatures the entropic contribution to the free energy increases, so eventually water elimination, which increases the entropy, becomes favorable despite being endothermic. In general, hydrothermal organic reactions tend to be controlled by thermodynamics and entropy, as opposed to kinetics and enthalpy, which are the primary controlling factors closer to ambient conditions. Both ionic and radical reaction mechanisms can occur simultaneously under hydrothermal conditions, although it is generally thought that ionic reactions are

Received: April 22, 2014
Published: July 15, 2014

Scheme 1. Schematic Representation of Functional Group Interconversions That Connect Simple Hydrocarbons and Carboxylic Acids, Proposed by Seewald for Hydrothermal Organic Reactions[7,18]

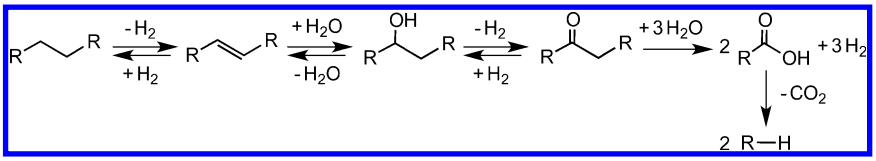

more prevalent at lower temperatures whereas radical reactions dominate at higher temperatures.[13]

Although many hydrothermal organic reactions have now been studied, the emphasis has been mainly on product distributions; mechanistic studies are less frequent, and direct evidence for proposed intermediates is often lacking. Partly this is because hydrothermal reactions can give complex product mixtures.[7,8,10,14,15] Other than kinetic measurements[16] and in some cases isotope effects,[17] the mechanistic toolbox for hydrothermal organic reactions is somewhat limited. One of the goals of this work was to develop a new experimental probe for hydrothermal organic reaction mechanisms.

The most abundant organic functional groups found in geochemical environments are alkanes and carboxylic acids.[7] Seewald has proposed a reaction scheme that shows how acids and alkanes might be connected by a series of reversible and irreversible functional group interconversions (Scheme 1).[7,18] The critical structure in this scheme is the ketone, since this is where irreversible carbon−carbon bond cleavage must occur. We recently studied the hydrothermal reactions of the model compound dibenzyl ketone (**DBK**) in order to investigate how bond cleavage might compete with functional group interconversions.[14] At 300 °C and 700 bar, all of the reactions in Scheme 1 were observed, except that carbon−carbon bond cleavage gave mainly coupling products rather than carboxylic acids.[14] The coupling products were explained as arising from homolytic bond cleavage to give primary benzyl and phenacyl radicals followed by rapid decarbonylation to give a pair of benzyl radicals (eq 1), although the observed coupling products

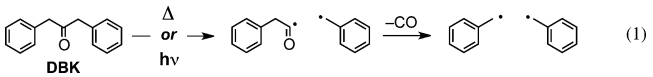

(1)

and their distributions were very different from those expected on the basis of the known **DBK**-derived radical chemistry under ambient conditions.[19] We thus sought independent evidence for the intermediacy of radicals in the bond cleavage reactions of **DBK** under hydrothermal conditions.

The ambient photochemistry of **DBK** and its analogues has been extensively studied in a variety of reaction media,[19] and the primary photophysical and chemical processes are well-established. Specifically, photochemical excitation of **DBK** ($h\nu$ in eq 1) gives the same primary radicals as previously proposed in the hydrothermal reactions of **DBK** (Δ in eq 1). Here we compare the thermal and photochemical reactions of **DBK** and show how independent generation of the primary radicals rationalizes the product distributions in the hydrothermal reactions of **DBK**. The photochemical method allows the primary radical coupling products to be identified. Because they are also formed on a much shorter time scale, their follow-up thermal reactions can be monitored directly. In short, hydrothermal photochemistry is found to be a very useful mechanistic tool for geochemically relevant hydrothermal reactions.

HYDROTHERMAL REACTIONS OF DBK

The hydrothermal decomposition reactions of **DBK** give a complex mixture of products that has been described in detail previously (Scheme 2).[14] One reaction pathway involves reduction, dehydration, and further reduction to give the corresponding alcohol (**2c**), alkene (**2d**), and alkane (**2e**) (although alcohol **2c** does not accumulate significantly because of rapid dehydration to form alkene **2d**), which corresponds to the functional group interconversion reactions shown in Scheme 1. The majority of the reaction products, however,

Scheme 2. Summary of the Main Products of the Hydrothermal Reaction of DBK at 300 °C and 700 bar[a]

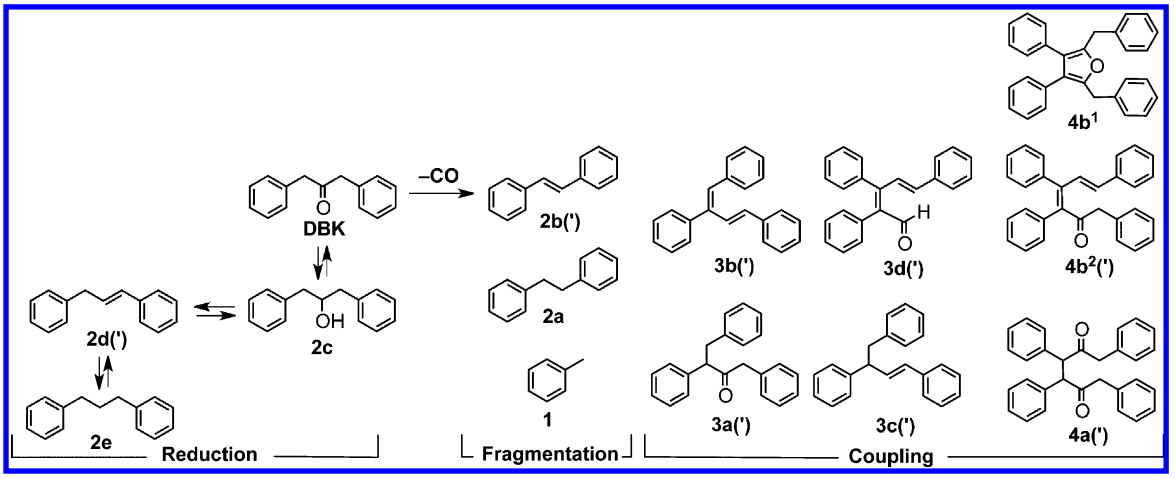

[a]From ref 14. Fragmentation and coupling reactions that give the products **1**, **2a**, **2b**, **3a−d**, **4a**, **4b**[1], and **4b**[2] compete with reduction and dehydration reactions that form alcohol **2c**, alkene **2d**, and alkane **2e**. The (′) symbol means that the product is formed in more than one stereoisomeric and/or structural isomeric form.

dx.doi.org/10.1021/jo500899x | J. Org. Chem. 2014, 79, 7861−7871

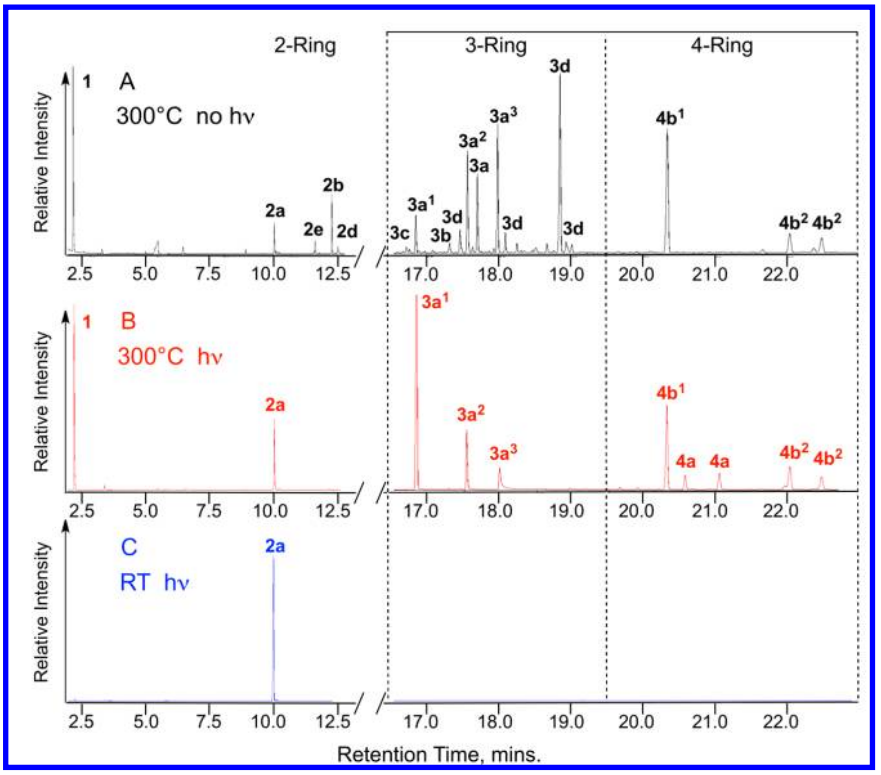

Figure 1. Gas chromatograms showing the product distributions for (**A**, black) the thermal reaction of **DBK** in water at 300 °C and 86 bar (no light) for a time period of 7 days, (**B**, red) hydrothermal photolysis in water at 300 °C and 86 bar for a time period of 33 min, and (**C**, blue) photolysis of **DBK** in methanol at room temperature (RT) for a time period of 33 min. The various products separate chromatographically into those that contain one, two, three, and four benzene rings.

are derived from carbon−carbon and carbon−hydrogen bond cleavage reactions and subsequent coupling processes, presumably via radical intermediates formed via eq 1.

Bibenzyl (**2a**) is an expected product of the coupling of two benzyl radicals, but it is formed in relatively low yield compared with other products. The various cleavage and coupling products are most easily categorized in terms of the number of benzene rings they contain: specifically, toluene (**1**) with one ring; bibenzyl (**2a**) and stilbene (**2b**) with two rings; and products that contain three benzene rings (**3a**−**d**) or four benzene rings (**4a** and **4b**) (Scheme 2).

Reactions designed to mimic geochemical conditions are often performed for extended time periods, and gold vessels are often used to minimize inadvertent catalysis by the reaction container. Gold is considered to be one of the more inert container materials.[20] Our previous experiments were performed in small, pressurized gold tubes, and because the photochemical reactions required the use of transparent fused-silica tubes, we first compared the reactions of **DBK** in fused-silica and gold.

Hydrothermal reactions of **DBK** were performed for 3 days in a fused silica tube, in a gold capsule that was sealed inside a fused-silica tube, and in a gold capsule with an external pressure of 700 bar. At 300 °C, the pressure in the fused-silica tube was determined to be ca. 86 bar (see the Experimental Section). At this pressure there was a headspace both in the fused-silica and the gold in fused silica tube experiments. Because gold is malleable, the external pressure of 700 bar was transmitted to the sample, and under these conditions there was no headspace. The observed products were identical in the three samples, although their distributions were slightly different. The **DBK** conversions were also somewhat different: 3.6%, 2.9%, and 2.1% in high-pressure gold, low-pressure gold, and fused silica, respectively. The conversions were slightly higher in gold, which suggests that the fused silica surface does not significantly catalyze the reaction.

A gas chromatogram showing the product distribution for a 7-day thermolysis experiment in a fused-silica tube is shown in Figure 1A. This longer reaction time period allows direct comparison to the photochemical experiments, but the product distribution is similar to that observed after 3 days.

HYDROTHERMAL PHOTOLYSIS OF DBK

1. Products of Hydrothermal Photolysis. The products of the 7 day, 300 °C hydrothermal reaction were compared with those for 33 min hydrothermal photolysis at 300 °C and also room-temperature photolysis in methanol. The conversions were low (5−8%) to minimize secondary reactions. In agreement with the earlier literature,[19] the photochemical reaction of **DBK** at room temperature yields bibenzyl (**2a**) as the only detectable product (Figure 1C). Hydrothermal photolysis at 300 °C, however, gives a very different product distribution (Figure 1B). Although bibenzyl is still observed, the major products are now toluene (**1**) and some of the three- and four-benzene-ring coupling products shown in Scheme 2. The product distribution from hydrothermal photolysis (Figure 1B) resembles a simpler version of the 7 day pure thermal reaction (Figure 1A). The hydrothermal photochemical conversion of **DBK** is linear with time, as is formation of toluene, bibenzyl, and the coupling products. Figure 2 shows the product yields as functions of irradiation time for the hydrothermal photochemical reaction compared with the corresponding reaction in methanol at room temperature,

dx.doi.org/10.1021/jo500899x | J. Org. Chem. 2014, 79, 7861−7871

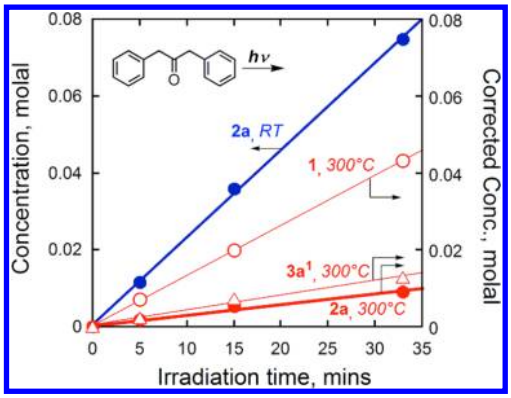

Figure 2. Comparison of product concentrations vs irradiation time for the photolysis of **DBK**, showing the formation of bibenzyl **2a** (blue ●) as the only product in methanol at RT and the formation of bibenzyl **2a** (red ●), toluene **1** (red ○), and the three-ring coupling product **3a**[1] (red △) in water at 300 °C and 86 bar. The concentrations of the products at 300 °C are corrected for the different conversions of **DBK** at the two reaction temperatures to allow direct comparison of the relative chemical yields at the two temperatures.

corrected for the different **DBK** conversions under the two conditions. This plot clearly shows the large difference in the product distributions under the two sets of conditions.

A mechanism that accounts for the fragmentation and coupling products for both the pure hydrothermal and photochemical hydrothermal reactions is shown in Scheme 3. The first steps are those in eq 1. Excitation of **DBK** to the first excited singlet state is followed by intersystem crossing (ISC) to the excited triplet state, which undergoes efficient homolytic bond cleavage to form a geminate benzyl/phenacyl radical pair. From the previously measured activation parameters,[21] decarbonylation of the phenacyl radical to yield another benzyl radical should occur in less than 2 ns at 300 °C. The geminate benzyl radical pair is formed in an overall triplet state, and efficient diffusive separation of this primary radical pair is expected to occur in fluid solution since recombination is spin-forbidden.[22] The pure thermal reaction forms the same geminate benzyl/phenacyl radical pair, in this case in an overall singlet spin state. Separated benzyl radicals then form by decarbonylation and diffusive separation.

The hydrothermal reaction of the benzyl radicals that does not take place under ambient conditions is hydrogen atom abstraction from **DBK** to yield toluene (**1**) and a **DBK**-derived radical, **DBK**• (shown as the process "H-abs" in Scheme 3). Coupling of **DBK**• with a benzyl radical generates the primary three-ring structures **3a**, which form as a mixture of three structural isomers. Coupling of two **DBK**• generates the primary four-ring structures **4a** (two stereoisomers are formed), which undergo thermal dehydration to form isomeric structures **4b**. The primary products of the hydrothermal photochemical radical reactions are thus **1** (toluene), **2a** (bibenzyl), **3a**, and **4a** (Scheme 3).

The hydrogen atom abstraction process (H-abs) occurs *in competition* with the conventional benzyl radical coupling to form bibenzyl (**2a**). Therefore, changing the relative rates of the competing processes should influence the product distribution. The formation of bibenzyl is kinetically second-order with respect to benzyl radical concentration, whereas the competing hydrogen atom abstraction with **DBK** is pseudo-first-order. The relative rates of these reactions should thus depend upon the radical concentration. Experiments were performed at higher light intensities where the radical concentration is higher. Under these conditions, the yield of bibenzyl increased compared with those of the coupling products, consistent

Scheme 3. Proposed Mechanism for the Formation of the Fragmentation and Coupling Products of the Hydrothermal Reaction of DBK at 300 °C[a]

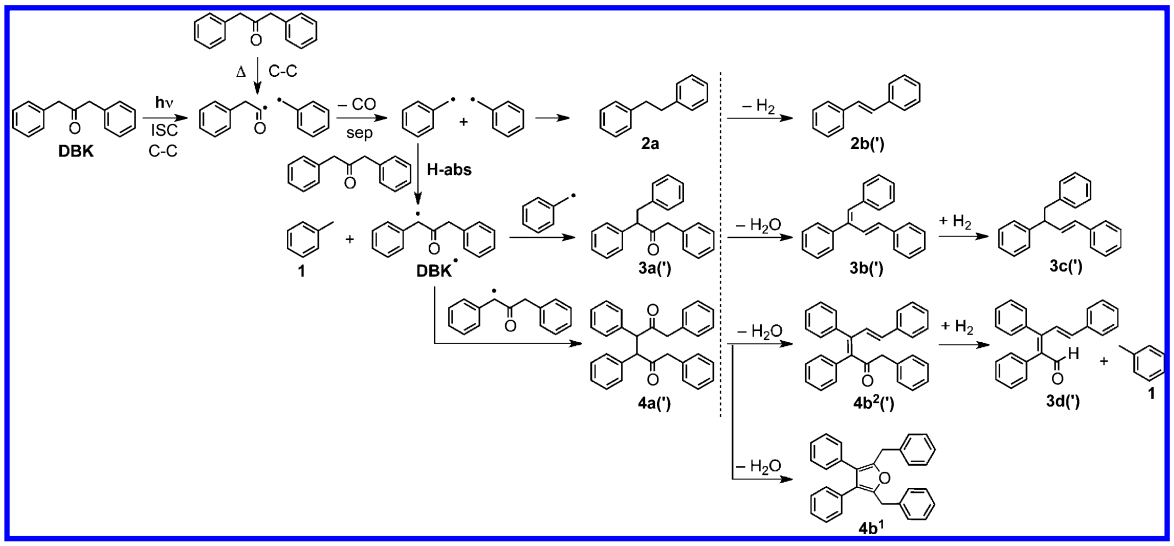

[a]The steps to the left of the dotted line are the radical processes, while those to the right of the dotted line are the follow-up thermal reactions that are mainly ionic. The first step in the photochemical reaction combines excitation of **DBK** to the first singlet state ($h\nu$), ISC to the triplet state, and finally homolytic cleavage (C–C) to form a benzyl radical and a phenacyl radical. This radical pair is also formed in the thermal (non-photochemical) reaction (Δ), although much more slowly and in an overall singlet state. The second step (–CO/sep) includes decarbonylation (–CO) and separation of the radicals in the geminate pair (sep). These primary steps are those given in eq 1. A separated benzyl radical reacts with **DBK** via hydrogen atom abstraction (H-abs) to yield toluene and a **DBK**-derived radical, **DBK**•. The (′) symbol associated with a structure indicates that more than one stereoisomer or structural isomer is formed.

dx.doi.org/10.1021/jo500899x | J. Org. Chem. 2014, 79, 7861–7871

with competing radical coupling and hydrogen atom abstraction.

Support for the mechanism shown in Scheme 3 was also obtained from experiments performed in the presence of Cu(II) ion, which is known to trap benzyl radicals via oxidation.[23] Hydrothermal photolysis of **DBK** was performed in the presence of 0.5 molal Cu(II) chloride for 15 min. The extent of **DBK** conversion was similar to that without Cu(II), but the yields of all of the radical products (**1**, **2a**, **3a**, and **4a**) were dramatically reduced by 80−90%. New oxidized products were detected in the presence of Cu(II), including benzaldehyde, benzoic acid, and phenylacetic acid. This provides strong evidence that benzyl and benzylic radicals are the precursors of the various coupling products of the hydrothermal photochemistry of **DBK**.

2. Relative Product Yields Support the Reaction Scheme. According to Scheme 3, one molecule of toluene is formed for each one of the three-ring coupling structures, and two molecules of toluene are formed for each one of the four-ring coupling structures. Therefore, the concentration of toluene in the product mixture, [**1**], should be equal to the sum of the concentrations of all of the three-ring products ($\sum$[3-ring]) plus twice the sum of the concentrations of all of the four-ring structures ($\sum$[4-ring]) (eq 2):

$$[\mathbf{1}] = \sum[\text{3-ring}] + 2\sum[\text{4-ring}] \quad (2)$$

The two sides of eq 2 are plotted as functions of time in Figure 3. The slopes of the plots are very similar, supporting eq 2 and

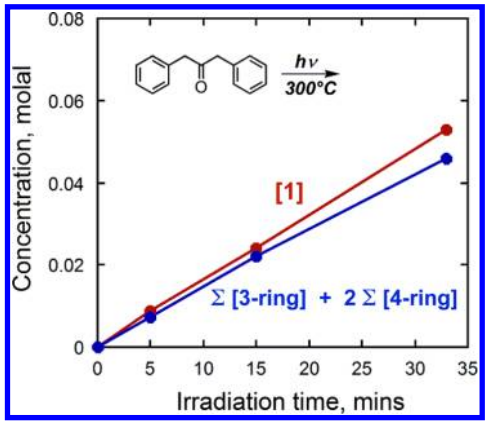

Figure 3. Time dependence of the concentration of toluene, [**1**], compared to that of the sum of the concentrations of 3-ring products plus twice the sum of the concentration of the 4-ring products. These should be equal according to eq 2; the small difference may be a consequence of assumed gas chromatography response factors for the coupling products (see the Supporting Information) or other experimental uncertainties.

the mechanism shown in Scheme 3. The small differences in the slopes are probably consequences of the assumptions for the gas chromatography response factors for the various coupling products (i.e., 1.5 and 2.0 times larger than for **DBK** for the three and four ring structures, respectively).

3. Relative Quantum Yields Support the Reaction Scheme. The formation of toluene and the coupling products requires consumption of more than one **DBK** molecule per absorbed photon. The quantum yield for bibenzyl formation in the ambient photochemistry of **DBK** is ca. 0.7, is essentially solvent-independent, and is the same as that for formation of separated benzyl radicals, since all of the separated benzyl radicals form coupling products.[19] According to Scheme 3, the formation of a three-ring coupling product and the accompanying toluene consumes two **DBK** molecules, while the formation of a four-ring product and the accompanying two toluenes consumes three **DBK** molecules. Thus, compared with the quantum yield for formation of bibenzyl, the quantum yields for the formation of the three-ring and four-ring structures should be 2 and 3 times larger, respectively. On the basis of the relative chemical yields of bibenzyl and the three- and four-ring structures, the quantum yield for **DBK** consumption under hydrothermal conditions can thus be calculated relative to conditions where bibenzyl is the only product.

Bibenzyl formation does not depend upon the **DBK** concentration, whereas the hydrogen atom abstraction reaction is pseudo-first-order with respect to **DBK**. It was found that the product distributions could also be varied controllably by changing the **DBK** concentration. Hydrothermal photolysis of **DBK** at a concentration of 0.05 molal gave bibenzyl as the major product, whereas at 1 molal concentration toluene and the coupling products dominated the distribution. The quantum yields for formation of the coupling products can thus be obtained by comparing experiments at different concentrations of **DBK**.

Hydrothermal photolyses of **DBK** at 0.05 molal and 1.0 molal were compared with the ambient photolysis of **DBK**, where bibenzyl was the only product, and at concentrations that had the same light absorption as the two hydrothermal samples (details are given in the Supporting Information). It was found that the **DBK** consumption for hydrothermal photolysis is higher per absorbed photon at the higher **DBK** concentration by a factor of ca. 1.3 compared with the lower concentration. The calculated hydrothermal quantum yield at 1 molal concentration, based on the observed product distribution and assuming that each of the three- and four-ring structures consumes two and three **DBK** molecules, respectively, is 1.37, which agrees quite well with the experimentally determined difference. The relative quantum yields thus also support the mechanism shown in Scheme 3.

4. Hydrogen Atom Abstraction. The critical step in the hydrothermal reaction mechanism is hydrogen atom abstraction from **DBK** by benzyl radicals. This process is responsible for the new products and is also responsible for consumption of more than one **DBK** molecule per photon. H atom abstraction does not occur under ambient conditions, so we examined this reaction computationally to see whether the reaction barrier could account for the different behaviors observed at the two temperatures. Methyl benzyl ketone (**MBK**) was studied instead of **DBK** for computational economy, using B3LYP/aug-cc-pVDZ as implemented in Gaussian 09.[24] **MBK** was optimized both in the gas phase and in solvent [modeled using the polarizable continuum model (PCM)] at 300 °C and 700 bar. Starting with the optimal conformer, the benzyl radical was fixed at 2.5 Å from the α-hydrogen of **MBK** (Figure 4), and the distance-constrained complex was fully optimized. From this geometry, the distance to the benzylic carbon of the radical, $C_{benzyl}-H_{\alpha}$, was shortened to 1.5 Å in steps of 0.1 Å and then to 1.35 Å in steps of 0.05 Å (with optimization of the distance-constrained complex at each step), at which point the $C_{\alpha}-H_{\alpha}$ bond separation distance in **MBK** became quite large (>3 Å), consistent with breaking of this bond. A search for the transition state located an extremely steep apex to the reaction coordinate (Figure 4). The transition-state structure was

dx.doi.org/10.1021/jo500899x | J. Org. Chem. 2014, 79, 7861−7871

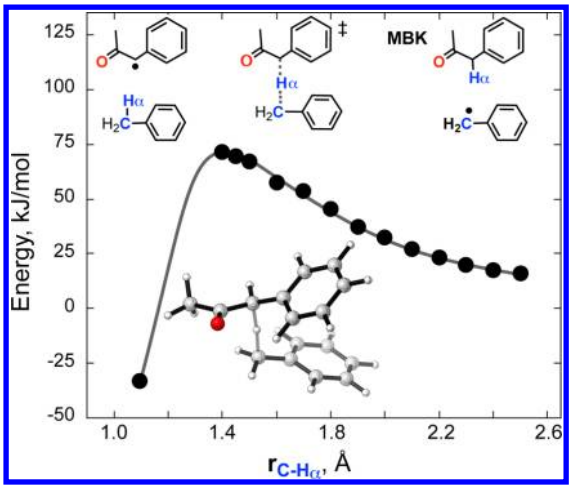

Figure 4. Electronic energy vs the α-hydrogen−benzylic carbon separation distance, $r_{C-H\alpha}$, for hydrogen atom abstraction from methyl benzyl ketone (**MBK**) by a benzyl radical. The inset shows the transition-state structure, located at $r_{C-H\alpha}$ = 1.41 Å, as computed using B3LYP/aug-cc-pVDZ and PCM to model the solvent. The energies are referenced to **MBK** + benzyl radical at an infinite separation distance. The reaction was computed to be exothermic by 29 kJ/mol at 300 °C and 700 bar. The computed free energy barrier for the reaction is 132 kJ/mol at 300 °C and 700 bar.

characterized by an associated imaginary vibrational frequency of 1528 cm^{-1}, which corresponds to the desired hydrogen transfer motion. The decrease in energy after the transition state is reached is artificially steep as a consequence of constraining only the $C_{benzyl}-H_\alpha$ coordinate and none of the other relevant bond distances. The reaction was found to be exothermic, as expected for a reaction that generates a more resonance-stabilized radical, by a value of 29 kJ/mol. This is in excellent agreement with the difference of 30 kJ/mol in the experimentally measured $C_{benzyl}-H_\alpha$ and $C_\alpha-H_\alpha$ bond dissociation energies [i.e., 377 kJ/mol for the benzylic C−H bond in toluene[25] and 347 kJ/mol for the benzylic (α) C−H bond in **MBK**;[26] bond dissociation enthalpies are essentially independent of temperature[25]]. The activation free energy was computed to be 132.4 kJ/mol at 300 °C, which translates into a bimolecular rate constant of 10.3 M^{-1} s^{-1} using transition state theory.[27] The corresponding activation energy and rate constant under ambient conditions were calculated to be 119.0 kJ/mol and 8.9 × 10^{-9} M^{-1} s^{-1}, respectively, indicating that the reaction is ca. 10^9 times slower than at 300 °C. This is consistent with bibenzyl being the only observable product at room temperature and H atom abstraction being competitive with radical recombination at 300 °C.

5. Characterization of the Coupling Products. Three structural isomers assigned to the coupling products **3a** are observed in the gas chromatogram/mass spectrum of the product mixture from hydrothermal photolysis. One of these isomers, corresponding to the peak with the shortest retention time in Figure 1B, is formed in significantly higher yield than the other two. These products are not isolable (the conversions are low, and the reaction mixtures are complex), and therefore, we can only make tentative assignments. Coupling of a benzyl radical and a **DBK**• radical could in principle occur at various positions since the spins are delocalized. For benzyl radical, the measured spin densities are 3.19, 1.0, and 1.22 for the benzylic, *ortho*, and *para* positions, respectively.[28] These spin densities do not explain the coupling of two benzyl radicals under ambient conditions in fluid solution, since coupling occurs only at the benzylic position. This is readily understood, since coupling at other positions initially forms a structure that has lost aromaticity. On this basis, we anticipate that the major product of the reaction of a benzyl radical and a **DBK**• radical would arise from coupling at the two benzylic positions to yield structure **3a**^{1} (shown in Schemes 3 and 4). However, non-benzylic coupling has occasionally been observed in photochemical reactions of **DBK** under ambient conditions in nonhomogeneous environments.[29] The equivalent non-benzylic coupling processes, shown in eqs 3a and 3b, yield structures that are tentatively assigned to the peaks **3a**^{2} and **3a**^{3} in Figure 1B (also see Scheme 4). The structures assigned to **3a**^{2} and **3a**^{3} in eqs 3 and Scheme 4 are shown as *para*-coupling isomers, although *ortho*-coupling isomers could also be formed and not be detected if they did not separate well under the chromatography conditions. **3a**^{2} and **3a**^{3} are formed in lower yields than **3a**^{1}, which is understandable since according to eqs 3 they must be formed via intermediates that have lost aromaticity. Formation of these non-benzylic coupling products under hydrothermal conditions points to higher reactivity and lower selectivity in the reactions of benzylic radicals at higher temperatures.

Scheme 4. Structural Isomers Assigned as Products of Benzyl/DBK Radical (DBK•) Coupling Observed in the Gas Chromatogram of Figure 1B[a]

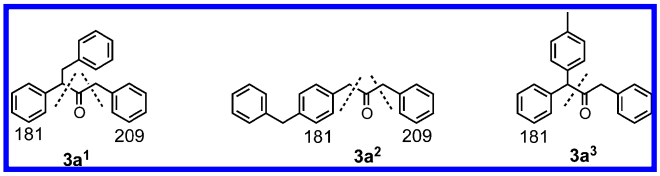

[a]The major product is assigned as **3a**^{1}. The products **3a**^{2} and **3a**^{3} are shown as *para*-coupling isomers, although *ortho*-coupling structures could also form. The dashed lines indicate the bonds that cleave to yield fragments with the indicated m/z values. For **3a**^{3}, the m/z 181 peak in the mass spectrum is much larger that the m/z 209 peak.

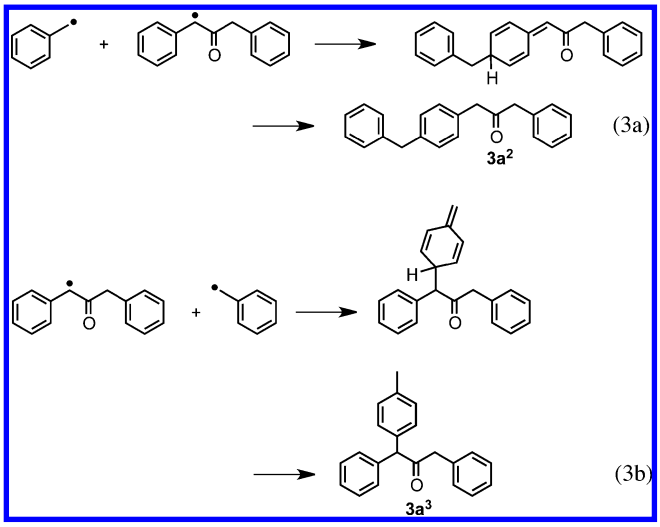

The assignments of **3a**^{1}, **3a**^{2}, and **3a**^{3} to the first, second, and third peaks, respectively, in the gas chromatogram of Figure 1B is supported by their mass spectra and also the observed follow-up thermal chemistry discussed below. The mass spectra for the peaks assigned to **3a**^{1} and **3a**^{2} are very similar and contain

dx.doi.org/10.1021/jo500899x | J. Org. Chem. 2014, 79, 7861−7871

fragments of similar size (m/z 181 and 209), consistent with cleavage on both sides of the carbonyl group to give benzyl ions (Scheme 4). In the mass spectrum for the peak assigned to **3a**[3], however, the m/z 209 peak is small and the m/z 181 peak is the base peak, since in the case of **3a**[3] the m/z 181 peak corresponds to a more stable diarylmethyl ion (see the Supporting Information).

Five products assigned to structures that contain four benzene rings are formed at early reaction times in sufficient quantities for mass spectral analysis (Figure 1B). Unlike the three-ring products, the time dependences of the concentrations of these structures are nonlinear (Figure 5). Two of

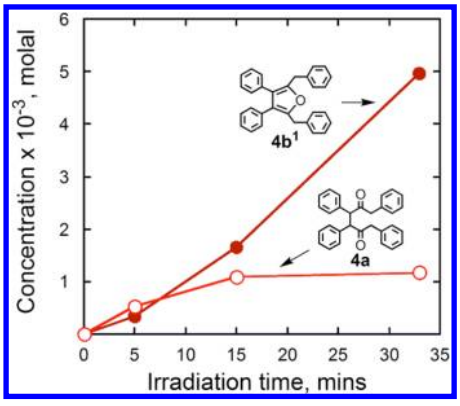

Figure 5. Concentration vs time plot for the photolysis of **DBK** in water at 300 °C at 86 bar for (○) the primary coupling product **4a** with the shorter retention time of the two diastereomers in Figure 1B and (●) the dehydrated four-ring product **4b**[1].

these structures are formed in equal abundance and have identical mass spectra, suggesting that they are the *meso*/(*d*,*l*) diastereomeric pair formed by coupling of two **DBK**• radicals (indicated as peaks **4a** in Figure 1B; the structure is shown in Scheme 3). The other four-ring products **4b**[1] and **4b**[2] indicated in Figure 1B are isomers with a molecular ion peak at m/z 400, consistent with formal loss of water compared with the **4a** isomers (Scheme 3). The rate of formation of the **4b** isomers increases as a function of irradiation time (Figure 5), consistent with the formation of the **4b** isomers by secondary thermal dehydration reactions of the **4a** isomers.

That **4b**[1] and **4b**[2] are derived from **4a** was readily demonstrated by an experiment in which hydrothermal photolysis was *followed* by thermolysis without light at 300 °C for a further 30 min. In this experiment it was found that the two peaks formed in the initial photolysis and assigned to the **4a** isomers had completely disappeared in a follow-up thermal reaction and that the peaks assigned to the **4b** isomers were correspondingly larger. This explains the nonlinear behavior of the **4a** and **4b**[1] concentrations with time shown in Figure 5.

FOLLOW-UP IONIC REACTIONS

In addition to providing insight into the thermal radical reactions, the photochemical technique allows the follow-up ionic thermal reactions to be more readily studied. The photochemical reaction clearly shows that the primary three-ring and four-ring radical coupling products are the **3a** and **4a** isomers. It was impossible to identify these primary products in the thermal-only experiment because of the simultaneous formation of secondary products.[14] In the thermal-only reactions, the primary three-ring products **3a** are not among the most abundant, and the primary four-ring products **4a** are not even observed (Figure 1A). The secondary products can be understood as arising from follow-up dehydration reactions of the **3a** and **4a** isomers. It should be noted that dehydration occurs efficiently despite the fact that the solvent is water and there are no added reagents or catalysts.

Dehydration of alcohols is perhaps the best-characterized hydrothermal reaction from a mechanistic perspective.[11,12] This reaction proceeds by acid-catalyzed elimination, with the water acting as the acid catalyst. It is well-known that under hydrothermal conditions K_w for water increases[30] and the dielectric constant of water decreases,[30] and with the increased thermal energy, the reactivity of the hydronium and hydroxide ions should increase. The mechanisms of the dehydration reactions of the ketones **3a** and **4a** are not as obvious, however, since these are not alcohols.

Further photolysis-followed-by-thermolysis experiments were performed in order to obtain a quantitative description of the dehydration reactions of **3a** and **4a**. Photolysis was performed at 300 °C for 2 min, followed by thermolysis at the same temperature for variable time periods. The rates of follow-up thermal dehydration were found to be very different for the **3a** isomers and the **4a** isomers. The reactions of both diastereomers of **4a** were complete within ca. 15 min after the light was shut off (both reacted at the same rate), whereas the reactions of the **3a** isomers were much slower. The different isomers of **3a** decreased in concentration at different rates, but none decreased by more than a factor of ca. 2 over a period of 1 day. The reactions of the **3a** isomers were so slow that accurate measurement of their reaction kinetics was not possible, since they were also being formed by thermal (non-photochemical) decomposition of **DBK** in the postphotolysis thermal reaction period. However, the kinetics of the conversions of the diastereomers of **4a** to the **4b** isomers were readily measured by quenching of photolysis samples after different follow-up thermolysis periods (Figure 6). Dehydration of the **4a** isomers to the **4b** isomers was remarkably fast: the pseudo-first-order

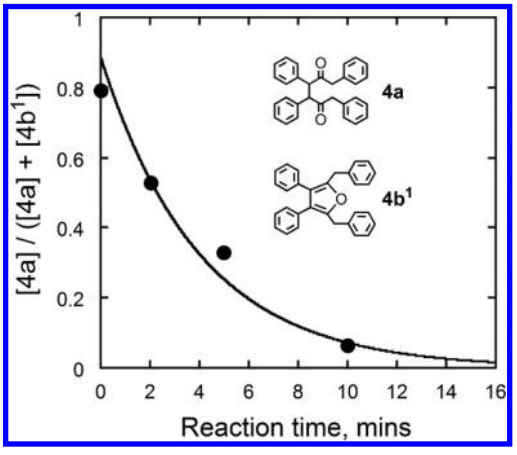

Figure 6. Time dependence of the concentration of **4a** (expressed as a fraction of the sum of the **4a** and **4b**[1] concentrations) in the dehydration reaction of **4a** to form furan **4b**[1] in water at 300 °C and 86 bar. The **4a** stereoisomer is the one with the shorter gas chromatographic retention time in Figure 1B. **4a** was formed by hydrothermal photolysis of **DBK** for 2 min, and this was followed by thermal dehydration for the various times indicated in the graph. The curve through the data corresponds to a pseudo-first order rate constant of 0.25 min^{-1}.

dx.doi.org/10.1021/jo500899x | J. Org. Chem. 2014, 79, 7861−7871

Scheme 5. Proposed Mechanisms for Brønsted Acid-Catalyzed Dehydrations of 3a and 4a To Give 3b(′) and 4b^1 or 4b^2(′), Respectively, via Enol [3e(′) and 4e(′)] and Conjugated Alkene [3f(′) and 4f(′)] Intermediates[a]

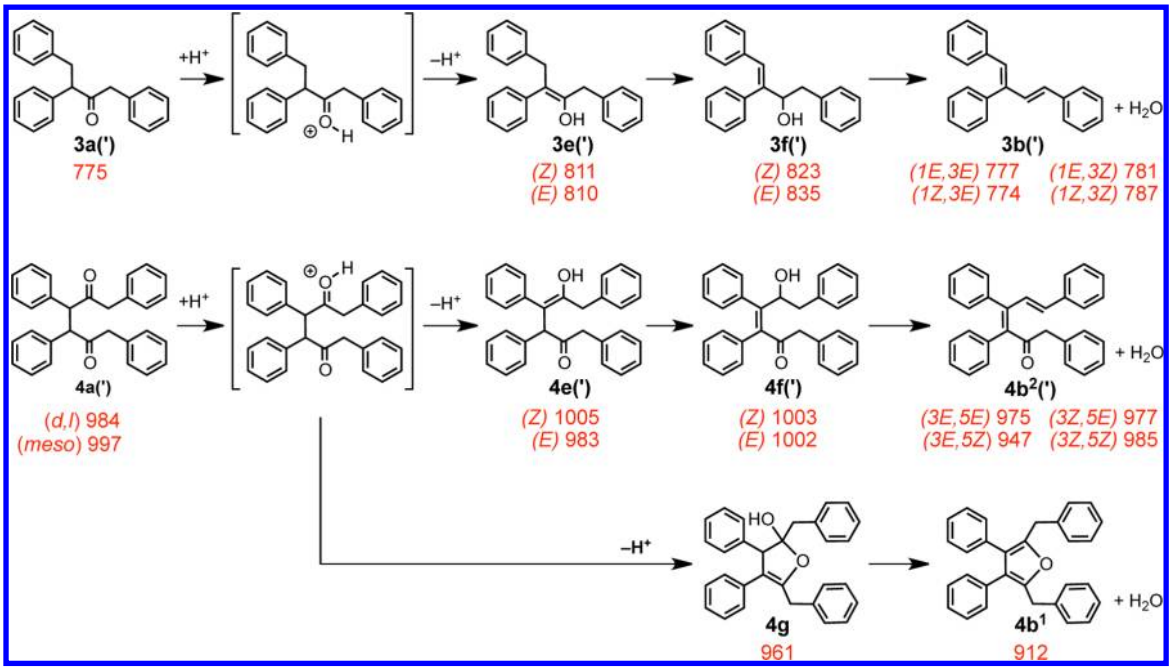

[a]The (′) symbol indicates stereoisomers and/or structural isomers. Acid can catalyze each step; only the first protonated intermediate is shown. Cyclization of the primary protonated intermediate is possible for **4a** (but not for **3a**) to give furan **4b^1**, a structural isomer of dienones **4b^2**(′). The numbers in red are the heats of formation in kJ/mol at 300 °C and 700 bar, calculated using the PM6 method with the solvent modeled using PMC as detailed in the Supporting Information. The values for **3b**(′), **4b^2**(′), and **4b^1** include the heat of formation of the water that is liberated in the last reaction, which is calculated to be −271 kJ/mol using the PM6/PCM method. Furan **4b^1** was calculated to be more stable than the corresponding dienones **4b^2**(′) by ca. 60 kJ/mol under these conditions using this method.

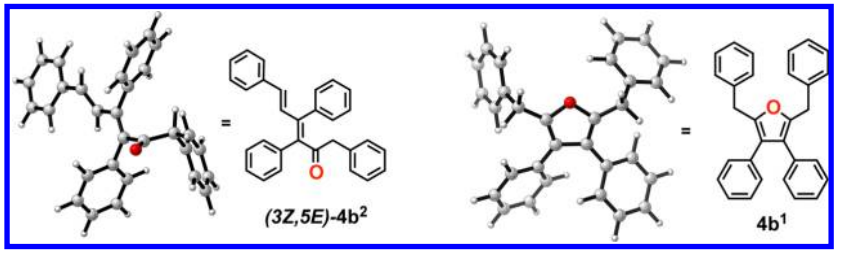

Figure 7. Structures of (left) the (3*Z*,5*E*) isomer of dienone **4b^2** and (right) the furan **4b^1** computed using the semiempirical PM6 method with PCM to model water as the solvent. The structures show a lack of planarity and lack of conjugation between the carbon−carbon and carbon−oxygen double bonds in the dienone and increased planarity in the furan.

rate constant is ca. 0.25 min^{-1}. It is clear that the reactivities of the **3a** and **4a** isomers are very different and that any proposed dehydration mechanism needs to account for this difference in reactivity.

We investigated possible acid-catalyzed dehydration reactions computationally. For these large structures, the semiempirical PM6 method was selected.[24,31] Calculations were performed at 300 °C and 700 bar (the conditions of the original gold tube experiments of ref 14) in simulated hot pressurized water using the PCM (details are provided in the Supporting Information). A plausible mechanism for the dehydration of **4a**/**3a** involves protonation of a carbonyl followed by formation of the corresponding enol (**4e**/**3e**), rearrangement to form an alcohol (**4f**/**3f**), and conventional acid-catalyzed elimination of water to generate the dienone/diene (**4b^2**/**3b**) (Scheme 5). Most of these structures could be formed in multiple stereoisomeric or structural isomeric forms, as indicated by the (′) symbols in Scheme 5 and as observed in the final dehydration products **3b** and **4b^2** in the gas chromatograms in Figure 1.

Heats of formation for the relevant intermediate structures are summarized in Scheme 5. Formation of the enol was found to be slightly endothermic for both **3a** and **4a**, as expected, and the isomerization **3e**/**4e** to **3f**/**4f** was almost thermoneutral. Deprotonation of the initially protonated carbonyl may skip the enol and form the alcohols **3f**/**4f** directly, but the energy changes along the two reaction pathways to the dienes **3b** and the dienones **4b^2**, including the final dehydration step, are very similar and cannot account for the large observed difference in the reaction rates for **3a** and **4a**. The isomeric dienones **4b^2** shown in Scheme 5 are sterically congested, and extensive conjugation is not observed in any of the calculated structures (e.g., see Figure 7). This lack of conjugation due to steric crowding is also observed in the enol and alkene isomers **3e**/**4e** and **3f**/**4f**. The heats of formation of the four stereoisomers of the dienones **4b^2** were found to be similar, although the

dx.doi.org/10.1021/jo500899x | J. Org. Chem. 2014, 79, 7861−7871

(3*Z*,5*E*) isomer is the most stable computationally and is the least crowded (Figure 7). The uncertainty in the heats of formation of isomeric organic structures such as those in Scheme 5 has been estimated to be ca. 16 kJ/mol.[32] One of the products of dehydration of **4a** is formed in significantly higher yield than the others (Figure 1B). The energy of the (3*Z*,5*E*) isomer is lower than those of the others by ca. 30 kJ/mol (i.e., by more than the reported estimated uncertainty in the heats of formation), but this energy difference is not enough to account for the formation of this isomer in significantly higher abundance than the others. However, another dehydration pathway is available to **4a** that can form a product that is even more stable than the dienones.

Protonated **4a** can undergo the known Paal–Knorr cyclization to form a furan,[33] whereas the corresponding protonated **3a** cannot (Scheme 5). This additional reaction pathway readily accounts for the significantly increased rate of dehydration of **4a** compared with **3a**. The furan that would be formed, shown as structure **4b**^{1} in Scheme 5 and Figure 7, is a structural isomer of the dienones **4b**^{2} in Scheme 5. Computationally, this furan is found to be significantly more stable than the dienones (by ca. 60 kJ/mol at 300 °C and 700 bar), which in turn suggests that it is the major dehydration isomer observed with the shortest retention time in the gas chromatograms of Figure 1. Although still sterically congested, furan **4b**^{1} is more conjugated than the least hindered dienone (Figure 7), which presumably contributes to its increased stability.

Isomers are possible for the dienones but not for furan **4b**^{1}. Three dehydration isomers are clearly observed in the gas chromatograms shown in Figure 1, and smaller peaks due to other isomers can also be detected at longer reaction times. Dehydration may form all of the isomers, or interconversion among the dienone isomers could also occur via protonation and deprotonation reactions. The development of a true thermodynamic equilibrium among the various isomers is unlikely, however, as a result of further follow-up reactions of dienones **4b**^{2} as discussed below.

Studies of model reactions also support Scheme 5. Enolization of ketones **3a** and **4a** can be tested using **DBK** itself as a model. As mentioned above, we expect the inherent Brønsted acid and base catalytic activity in water to be high at 300 °C. The hydrothermal reaction of **DBK** in deuterated water at 300 °C for 10 min resulted in complete incorporation of four deuteriums in the unreacted **DBK**, as determined by mass spectrometry, presumably as a consequence of exchange of the four enolizable hydrogens in **DBK**.[34] Thus, enolization readily occurs on the time scale of the dehydration reaction. The second isomerization step can also be readily understood as proceeding via acid catalysis (protonation followed by deprotonation), similar to enolization (Scheme 5). That this process could also be fast on the time scale of the **4a** dehydration is supported by the calculated heats of formation, which indicate that the process **4e** → **4f** is even less endothermic than the enolization step, as well as observation of rapid interconversions among isomeric alkenes under similar conditions.[15]

The final step in the mechanism of Scheme 5 is dehydration of the alcohol, which we modeled by studying the same reaction in 1-phenylethanol (eq 4). Thermolysis of 1-phenylethanol in water for 1 h at 300 °C resulted in conversion of 50% of the alcohol to styrene. The mechanism of hydrothermal alcohol dehydration has previously been shown

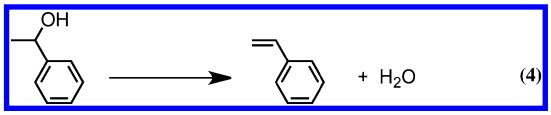

to proceed via protonation of the oxygen followed by conventional E1 or E2 elimination.[11,12] The rate of this dehydration is intermediate between those observed for the overall more complex dehydrations of **3a** and **4a**, suggesting that the reactions in Scheme 5 are plausible on the observed time scales.

SEPARATING THE IONIC AND RADICAL REACTION PATHWAYS

The photochemical reaction effectively separates the radical reactions from the mainly ionic secondary dehydration reactions that occur simultaneously with the radical reactions in the pure thermal reaction (Scheme 3). This separation allowed us to construct the reaction scheme for the formation of the fragmentation and coupling products (Scheme 3), which was not possible from the previous thermal-only studies.[14]

Hydrothermal photolysis followed by thermolysis eventually results in a product distribution resembling that of the pure thermolysis reaction (Figure 1A). As mentioned above, thermolysis after photolysis results in the complete removal of the **4a** isomers via dehydration. Thermolysis after photolysis does not completely remove the **3a** isomers, but their product distribution changes compared with that after short-time photolysis alone. In particular, the major product of hydrothermal photolysis, **3a**^{1}, becomes the least abundant of the **3a** isomers upon thermolysis, and additional three-ring structures are observed, although in greater yields than could be explained by reactions of **3a** alone.

This observation is explained by recognizing that **3a**^{1} can undergo the same dehydration reaction as **4a** to give **3b** isomers (Scheme 3). The structures assigned to **3a**^{2} and **3a**^{3}, however, cannot undergo corresponding dehydration but could in principle undergo reactions similar to those of **DBK** itself. Under the experimental conditions and time scales, conversion to secondary products would be expected to be minimal since the reactions of **DBK** itself are relatively slow.[14] Toluene (**1**) would be expected to be a major product of these reactions, but structural isomers of bibenzyl (**2a**) and other coupling products would also be expected to form eventually. In support of this, small peaks in the gas chromatograms, close to authentic bibenzyl, are observed upon extended thermolysis and appear to be bibenzyl isomers on the basis of mass spectral analysis (Figure 1).

After extended thermolysis, the major three-ring structure is aldehyde **3d**, which is formed as multiple stereoisomers (Scheme 3). We have not yet investigated this reaction in detail; however, the aldehyde yield after extended reaction times is sufficiently large that it cannot be formed from reactions of the primary three-ring products **3a**. A potential alternate source of **3d** is via bond homolysis in dienones **4b**^{2} (Scheme 3). The other product of this reaction would be toluene (**1**), although formation of **3d** and **1** from **4b**^{2} requires two hydrogen atoms. With extended reaction times, stilbene (**2b**, mainly the *trans* isomer) becomes a major product in the two-benzene-ring region at the expense of bibenzyl (Figure 1A). The conversion to stilbene from bibenzyl formally generates hydrogen atoms that could be used in the formation of **3d** from **4b**^{2}.

dx.doi.org/10.1021/jo500899x | J. Org. Chem. 2014, 79, 7861–7871

CONCLUSIONS

Hydrothermal photolysis of dibenzyl ketone allows the identification of the primary radical coupling products in the corresponding thermal reactions and reveals unexpected reactions of benzylic radicals in high-temperature water. Hydrothermal photolysis also allows separation of the radical and ionic reactions that occur simultaneously in the purely thermal experiment without photolysis. Reactions of the benzyl radicals at high temperature that do not occur under ambient conditions include *ortho* and *para* coupling and hydrogen atom abstraction from **DBK** itself. The increased thermal energy and increased K_w facilitate rapid Brønsted acid- and base-catalyzed reactions that are not observed under ambient conditions, specifically dehydration of the ketones **3a** and **4a**. Although alcohol dehydration has been observed many times in hydrothermal organic reactions, this work points to dehydration as a generally favorable process for different kinds of structures.[5] The follow-up reactions in Scheme 5 are mainly Brønsted acid-catalyzed, and it is well-known that natural geologic systems are characterized by widely varying pH and distributions of organic materials and functional groups.[35] Isolation of the ionic pH-dependent reactions is thus a valuable tool to aid in the understanding of the complex schemes that often characterize geologically relevant organic processes.

EXPERIMENTAL SECTION

Most of the chemicals were available from previous work.[14] Copper chloride (98%) was purchased from Sigma-Aldrich and used without purification. The hydrothermal photolysis experiments were carried out in fused silica glass tubes (GM Associates, Inc.) that had a 6 mm outside diameter and a 2 mm inside diameter. **DBK** was weighed into the tubes, and 0.2 mL of argon-purged deionized water was added to obtain solutions that, when heated, ranged in concentration from 0.035 to 1 molal. It was previously confirmed that **DBK** is soluble at all experimental concentrations at 300 °C.[14] The samples were frozen in liquid nitrogen, evacuated using three pump−freeze−thaw cycles, and sealed under vacuum with a hydrogen flame to a length of ∼12 cm. Each sample occupied ∼8 cm of the tube length at room temperature, and the remainder was evacuated headspace. The volume of the headspace was diminished by water expansion at 300 °C since the density of water decreases ca. 30% in going from room temperature to 300 °C. The pressure in the tube at 300 °C was determined to be ca. 86 bar using SUPCRT 92.[36] The sealed fused silica tubes were placed vertically in a large brass block that was heated using cartridge heaters. A thermocouple inside the brass block next to the sample tube was used to monitor the reaction temperature. The samples were preheated in the brass block at 300 °C for 5 min before irradiation for time periods of 2 to 33 min. The 5 min preheating time was established in an experiment where the temperature was measured directly using a thermocouple placed inside the same silica glass tube containing silicone oil. The light source was a 200 W mercury arc lamp (Osram HBO200W) equipped with an arc lamp power supply system (model 8500, Oriel, Stamford, CT, USA). A filter solution of potassium chromate and sodium carbonate was used to isolate the 313 nm emission line and control the light intensity.[37] After irradiation, the samples were immediately quenched in a cold-water bath.

For longer-time-scale (thermolysis only) experiments, the samples were heated in a gas chromatography oven at 300 °C for 3, 7, or 12 days. Thermolysis experiments in gold tubes at 300 °C and 700 bar were performed using the apparatus and methods described previously.[14] A low-pressure gold capsule hydrothermal experiment at 300 °C and 86 bar was performed by sealing a gold capsule inside a larger fused silica tube with a 12 mm outside diameter and a 6 mm inside diameter, which was placed in a Swagelok pipe that contained water to equalize the pressure inside and outside the fused silica tube and prevent fracture. Room-temperature photolyses of **DBK** were carried out in the same fused silica tubes and apparatus as the high-temperature photolysis experiments. Radical trapping experiments were performed using 0.5 molal $CuCl_2$ at 300 °C and 86 bar.

The extraction and analytical procedures were as described previously.[14] Gas chromatography with flame ionization detection (FID) was used for quantitative analysis of the reaction mixtures. Because of the low conversions and the number of products, it was not possible to isolate the coupling products containing three or four benzene rings. As described previously,[14] the gas chromatography FID response factors for these coupling structures were estimated on the basis of the number of benzene rings that they contained; specifically, the values for the three-benzene-ring and four-benzene-ring structures were estimated to be 1.5 and 2.0 times larger than that for **DBK**, respectively.

ASSOCIATED CONTENT

Supporting Information

Computational details, a description of the quantum yield experiments, mass spectra of the coupling products, and the full citation for ref 24 (as SI ref 5). This material is available free of charge via the Internet at http://pubs.acs.org.

AUTHOR INFORMATION

Corresponding Authors

*E-mail: lynda.williams@asu.edu.
*E-mail: h.hartnett@asu.edu.
*E-mail: everett.shock@asu.edu.
*E-mail: igould@asu.edu.

Notes

The authors declare no competing financial interest.

ACKNOWLEDGMENTS

This work was supported by National Science Foundation Grant OCE 0826588. We thank all of the members of the Hydrothermal Organic Geochemistry (HOG) Group at ASU for many stimulating discussions and helpful suggestions. We are also grateful to Pierre Herckes and Jinwei Zhang (Arizona State University) for their assistance with the GC−MS analysis.

DEDICATION

I.R.G. dedicates this manuscript to the memory of N. J. Turro, a master teacher and scholar, who used the photochemistry of dibenzyl ketone to teach the chemical community so much.

REFERENCES

(1) Falkowski, P.; Scholes, R. J.; Boyle, E.; Canadell, J.; Canfield, D.; Elser, J.; Gruber, N.; Hibbard, K.; Hogberg, P.; Linder, S.; Mackenzie, F. T.; Moore, B.; Pedersen, T.; Rosenthal, Y.; Seitzinger, S.; Smetacek, V.; Steffen, W. *Science* **2000**, *290*, 291−296.

(2) (a) Dasgupta, R. *Rev. Mineral. Geochem.* **2013**, *75*, 183−229. (b) Manning, C. E.; Shock, E. L.; Sverjensky, D. A. *Rev. Mineral. Geochem.* **2013**, *75*, 109−148.

(3) Helgeson, H. C.; Richard, L.; McKenzie, W. F.; Norton, D. L.; Schmitt, A. *Geochim. Cosmochim. Acta* **2009**, *73*, 594−695.

(4) Horsfield, B.; Schenk, H. J.; Zink, K.; Ondrak, R.; Dieckmann, V.; Kallmeyer, J.; Mangelsdorf, K.; di Primio, R.; Wilkes, H.; Parkes, R. J.; Fry, J.; Cragg, B. *Earth Planet. Sci. Lett.* **2006**, *246*, 55−69.

(5) Shock, E. L.; Canovas, P.; Yang, Z.; Boyer, G.; Johnson, K.; Robinson, K.; Fecteau, K.; Windman, T.; Cox, A. *Rev. Mineral. Geochem.* **2013**, *76*, 311−350.

(6) (a) Price, L. C.; DeWitt, E. *Geochim. Cosmochim. Acta* **2011**, *65*, 3791−3826. (b) Tassi, F.; Vaselli, O.; Capaccioni, B.; Montegrossi, G.; Barahona, F.; Caprai, A. *Geochem., Geophys., Geosyst.* **2007**, *8*, No. Q05008.

(7) (a) Seewald, J. S. *Nature* **2003**, *426*, 327−333. (b) McCollom, T. M.; Seewald, J. S. *Geochim. Cosmochim. Acta* **2003**, *67*, 3625−3644. (c) McCollom, T. M.; Seewald, J. S. *Geochim. Cosmochim. Acta* **2003**, *67*, 3645−3664.
(8) For example, see: (a) Siskin, M.; Katritzky, A. R. *Science* **1991**, *254*, 231−237. (b) Katritzky, A. R.; Nichols, D. A.; Siskin, M.; Murugan, R.; Balasubramanian, M. *Chem. Rev.* **2001**, *101*, 837−892. (c) Siskin, M.; Katritzky, A. R. *Chem. Rev.* **2001**, *101*, 826−835. (d) Akiya, N.; Savage, P. E. *Chem. Rev.* **2002**, *102*, 2725−2750. (e) Hunter, S. E.; Savage, P. E. *Chem. Eng. Sci.* **2004**, *59*, 4903−4909. (f) Watanabe, M.; Sato, T.; Inomata, H.; Smith, R. L.; Arai, K.; Kruse, A.; Dinjus, E. *Chem. Rev.* **2004**, *104*, 5803−5821.
(9) (a) Avola, S.; Guillot, M.; da Silva-Perez, D.; Pellet-Rostaing, S.; Kunz, W.; Goettmann, F. *Pure Appl. Chem.* **2013**, *85*, 89−103. (b) Shanab, K.; Neudorfer, C.; Schirmer, E.; Spreitzer, H. *Curr. Org. Chem.* **2013**, *17*, 1179−1187.
(10) (a) Seewald, J. S. *Nature* **1994**, *370*, 285−287. (b) Seewald, J. S.; Zolotov, M. Y.; McCollom, T. *Geochim. Cosmochim. Acta* **2006**, *70*, 446−460.
(11) (a) Shock, E. L. *Geochim. Cosmochim. Acta* **1993**, *57*, 3341−3349. (b) Xu, X.; Antal, M. J. *AIChE J.* **1994**, *40*, 1524−1534. (c) Xu, X.; Antal, M. J.; Anderson, D. G. M. *Ind. Eng. Chem. Res.* **1997**, *36*, 23−41. (d) Kuhlmann, B.; Arnett, E. M.; Siskin, M. *J. Org. Chem.* **1994**, *59*, 3098−3102. (e) Akiya, N.; Savage, P. E. *Ind. Eng. Chem. Res.* **2001**, *40*, 1822. (f) Ott, L.; Bicker, M.; Vogel, H. *Green Chem.* **2006**, *8*, 214−220.
(12) Antal, M. J.; Brittain, A.; DeAlmeida, C.; Ramayya, S.; Roy, J. C. *ACS Symp. Ser.* **1987**, *329*, 77−86.
(13) (a) LaRowe, D. E.; Van Cappellen, P. *Geochim. Cosmochim. Acta* **2011**, *75*, 2030−2042. (b) Burdige, D. J. *Geochemistry of Marine Sediments*; Princeton University Press: Princeton, NJ, 2006.
(14) Yang, Z.; Gould, I. R.; Williams, L. B.; Hartnett, H. E.; Shock, E. L. *Geochim. Cosmochim. Acta* **2012**, *98*, 48−65.
(15) Shipp, J.; Gould, I. R.; Herckes, P.; Shock, E. L.; Williams, L. B.; Hartnett, H. E. *Geochim. Cosmochim. Acta* **2013**, *104*, 194−209.
(16) For example, see: (a) Belsky, A. J.; Maiella, P. G.; Brill, T. B. *J. Phys. Chem. A* **1999**, *103*, 4253−4260. (b) Li, J.; Brill, T. B. *Int. J. Chem. Kinet.* **2003**, *35*, 602−610. (c) Li, J.; Brill, T. B. *J. Phys. Chem. A* **2001**, *105*, 6171−6175. (d) McCollum, T. M.; Seewald, J. S. *Geochim. Cosmochim. Acta* **2003**, *67*, 3645−3664.
(17) For example, see: (a) Hoering, T. C. *Org. Geochem.* **1984**, *5*, 267−278. (b) Yamamoto, M.; Yokota, Y.; Oshima, K.; Matsubara, S. *Chem. Commun.* **2004**, 1714−1715. (c) Matsubara, S.; Yokota, Y.; Oshima, K. *Org. Lett.* **2004**, *6*, 2071−2073. (d) McCollom, T. M.; Lollar, B. S.; Lacrampe-Couloume, G.; Seewald, J. S. *Geochim. Cosmochim. Acta* **2010**, *74*, 2717−2740. (e) Reeves, E. P.; Seewald, J. S.; Sylva, S. P. *Geochim. Cosmochim. Acta* **2012**, *77*, 582−599.
(18) Seewald, J. S. *Geochim. Cosmochim. Acta* **2001**, *65*, 1641−1664.
(19) (a) Robbins, W. K.; Eastman, R. H. *J. Am. Chem. Soc.* **1970**, *92*, 6076−6077. (b) Robbins, W. K.; Eastman, R. H. *J. Am. Chem. Soc.* **1970**, *92*, 6077−6079. (c) Turro, N. J. *Tetrahedron* **1982**, *38*, 809−817. (d) Gould, I. R.; Baretz, B. H.; Turro, N. J. *J. Phys. Chem.* **1987**, *91*, 925−929. (e) Garcia-Garibay, M. A.; Zhang, Z.; Turro, N. J. *J. Am. Chem. Soc.* **1991**, *113*, 6212−6218. (f) Turro, N. J. *Acc. Chem. Res.* **2000**, *33*, 637−646. (g) Warrier, M.; Turro, N. J.; Ramamurthy, V. *Tetrahedron Lett.* **2000**, *41*, 7163−7167.
(20) For example, see: Palmer, D. A.; Drummond, S. E. *Geochim. Cosmochim. Acta* **1986**, *50*, 813−823.
(21) (a) Turro, N. J.; Gould, I. R.; Baretz, B. H. *J. Phys. Chem.* **1983**, *87*, 531−532. (b) Lunazzi, L.; Ingold, K. U.; Scaiano, J. C. *J. Phys. Chem.* **1983**, *87*, 529−530.
(22) Gould, I. R.; Turro, N. J.; Zimmt, M. B. *Adv. Phys. Org. Chem.* **1984**, *20*, 1−51.
(23) Turro, N. J.; Weed, G. C. *J. Am. Chem. Soc.* **1983**, *105*, 1861−1868.
(24) Frisch, M. J.; et al. *Gaussian 09*, revision C.01; Gaussian, Inc.: Wallingford, CT, 2009.
(25) Blanksby, S. J.; Ellison, G. B. *Acc. Chem. Res.* **2003**, *36*, 255−263.
(26) Bordwell, F. G.; Harrelson, J. A. *Can. J. Chem.* **1990**, *68*, 1714−1718.
(27) Fernandez-Ramos, A.; Miller, J. A.; Klippenstein, S. J.; Truhlar, D. G. *Chem. Rev.* **2006**, *106*, 4518−4584.
(28) Dust, J. M.; Arnold, D. R. *J. Am. Chem. Soc.* **1983**, *105*, 1221−1227.
(29) For example, see: Lehr, G. F.; Turro, N. J. *Tetrahedron* **1981**, *37*, 3411−3420.
(30) Harvey, A. H.; Friend, D. G. In *Aqueous Systems at Elevated Temperatures and Pressures*; Palmer, D. A., Fernandez-Prini, R., Harvey, A. H., Eds.; Elsevier: San Diego, CA, 2004.
(31) Stewart, J. P. P. *J. Mol. Model.* **2007**, *13*, 1173−1213.
(32) Isegawa, M.; Fiedler, L.; Leverentz, H. R.; Wang, Y.; Nachimuthu, S.; Gao, J.; Truhlar, D. G. *J. Chem. Theory Comput.* **2013**, *9*, 33−45.
(33) Amarnath, V.; Amarnath, K. *J. Org. Chem.* **1995**, *60*, 301−307.
(34) For example, see: Siskin, M.; Katritzky, A. R.; Balasubramanian, M. *Fuel* **1995**, *74*, 1509−1511.
(35) McSween, H. Y.; Richardson, S. M.; Uhle, M. E. *Geochemistry: Pathways and Processes*, 2nd ed.; Columbia University Press: New York, 2003.
(36) Johnson, J. W.; Oelkers, E. H.; Helgeson, H. C. *Comput. Geosci.* **1993**, *18*, 899−947.
(37) Murov, S. L.; Carmichael, I.; Hug, G. L. *The Handbook of Photochemistry*, 2nd ed.; CRC Press: Boca Raton, FL, 1993.